Article

Impact of Extreme Weather Events on the Surface Energy Balance of the Low-Elevation Svalbard Glacier Aldegondabreen

Uliana V. Prokhorova [1,*], Anton V. Terekhov [1], Vasiliy E. Demidov [1], Kseniia V. Romashova [1], Kirill V. Barskov [2], Dmitry G. Chechin [2,3], Igor I. Vasilevich [1], Mikhail V. Tretiakov [1], Boris V. Ivanov [1,4], Irina A. Repina [2] and Sergey R. Verkulich [1]

[1] Arctic and Antarctic Research Institute, 199397 Saint Petersburg, Russia; antonvterekhov@gmail.com (A.V.T.); vasdemidov@mail.ru (V.E.D.); hydrology2@aari.ru (K.V.R.); vasilevich@aari.ru (I.I.V.); tmv@aari.ru (M.V.T.); b_ivanov@aari.ru (B.V.I.)

[2] Obukhov Institute of Atmospheric Physics of the Russian Academy of Sciences, 119017 Moscow, Russia; chechin@ifaran.ru (D.G.C.); iar.ifaran@gmail.com (I.A.R.)

[3] Moscow Center of Fundamental and Applied Mathematics, 119991 Moscow, Russia

[4] Institute of Earth Sciences, Saint Petersburg State University, 199034 Saint Petersburg, Russia

*   Correspondence: uvprokhorova@aari.ru

Abstract: The summer of 2022 was notable for the Svalbard archipelago due to the occurrence of several longstanding heatwaves, making it one of the warmest summers on the regional record. This study used an energy balance model forced with in situ weather observations to investigate the influence of extreme weather events on the surface energy balance of the low-elevation Aldegondabreen glacier (5.2 km^2), located near Barentsburg town, with a focus on the turbulent heat exchange. The annual mass balance for 2022 (-2.13 m w.e.) was one of the most negative on record for Aldegondabreen since 2002/2003 when glaciological monitoring was first initiated. We identified four heatwaves that lasted from 9 to 19 days, the most prominent of which were observed in May and in September–October, which resulted in an anomalously prolonged melt season. In addition, several shorter, 1- to 3-day extreme melt events were identified, representing up to 75 mm w.e. day^{-1} of glacier-averaged melt. These events were well correlated (r = 0.87, $p < 0.01$), with discharge from a stream originating from the glacier terminus, and all cases were associated with significant increases in mean daily wind speeds (up to 10.3 m s^{-1}).

Keywords: Arctic; Svalbard; energy balance; mass balance; glaciology; climate changes; modeling

1. Introduction

Svalbard is one of the fastest-warming regions of the world [1]; at the same time, it is one of the most glaciated areas in the Arctic, accounting for up to 10% of the total glaciated area outside Greenland. In the early 21st century, the archipelago-wide climatic mass balance was negative [2]; however, future projections indicate that the mass balance of Svalbard glaciation will continue to decline at an accelerated rate, potentially leading to the total disappearance of minor glacial bodies by the end of 21st century [3].

The surface energy balance (SEB) of the Svalbard glaciation has been relatively well studied. Previous studies have shown that the primary driver for glacial melt during the ablation period is short-wave solar radiation [4–6]. This is especially true for glaciers at lower elevations that are situated under the present-day snow line and, thus, are characterized by a significantly lower albedo during the melt period. In recent decades, the ablation zone on

Svalbard has widened, a trend that is likely to persist [7]. This may imply an increase in the sensitivity of Svalbard glaciation to variations in incident solar radiation.

On the time scale of the entire ablation season, the sum of the sensible and latent heat fluxes only accounted for about 10% of the total energy available for melting (e.g., [8]). In contrast, turbulent energy exchange cannot be assumed to be negligible; on synoptic time scales, sensible and latent heat fluxes may be drastically amplified by synoptic and mesoscale events, such as foehn winds and cyclonic activity [6,9]. Such phenomena may prolong ablation during autumn—when the solar radiative flux is low on Svalbard—by providing extra energy for glacier melt or preventing the accumulation of solid precipitation.

However, recent years have demonstrated another type of weather event that heavily influences glacier melt on a regional scale. It is predicted that due to ongoing climate change, heatwaves will occur more frequently in the near future and their duration will increase [10]. As a result, the impact of extreme weather events on the cryosphere is increasingly becoming a subject of research. Previously, the effects of individual heatwaves on glacier melt have been studied in Europe [11–13], in Asia [14], and for the American continent [15,16].

We present a similar study focusing on Svalbard, expanding on previous research by analyzing the impact of extreme weather events in this region. The year 2022 was notable for Svalbard and for the entire European subcontinent for the occurrence of several longstanding heatwaves [17]. The summer of 2022 was reported as the warmest on record in the Svalbard region at the time, with some areas experiencing temperatures more than 2.5 °C above the average [18]. However, our study extends beyond the analysis of heatwaves, as we also investigate the impact of extreme values of other meteorological variables—beyond air temperature—on the glacier SEB.

In this study, we attempt to quantify the impact of the extreme events of 2022 on the SEB of the low-elevation Svalbard glacier Aldegondabreen. We applied a spatially distributed 1 d energy balance model forced with in situ weather observations acquired on the Aldegondabreen glacier to produce time series data of its SEB components. The model was calibrated using the ice melt layer measured at the ablation stakes. The model output was then validated in two different ways: first, we compared the values of sensible heat flux computed from bulk aerodynamic formulas with those obtained from the eddy covariance method; second, we showed that apparent peaks in the turbulent heat exchange corresponded to peaks observed on a water-level gauge installed on a stream originating from the glacier. To assess the impact of heatwaves on the glacial mass balance, we computed the energy surplus during the extreme melt events relative to the corresponding climatic normals. These climatic normals were derived using a time series dataset obtained from the nearest station located in Barentsburg (10 km northeast) over a 30-year period between 1991 and 2020.

2. Materials and Methods

2.1. Study Site and Research Background

The Aldegondabreen glacier (77.971° N 14.072° E, area 5.2 km^2) is located in the western part of Nordenskiöld Land in the vicinity of Barentsburg town and occupies an elevation range between 125 and 500 m above sea level. Consequently, almost the entire surface of the glacier is located just below the altitude of the mean equilibrium line as recorded in recent decades [19]. A record of its glaciological mass balance has been tracked since the beginning of the 21st century, and it has been shown that the inter-annual mass balance variations of this glacier are reflective of the Barentsburg area and, in general, follow archipelago-wide trends, making it representative of low-elevation Svalbard glaciation [20].

The Svalbard archipelago is currently experiencing Arctic amplification (AA)—a prominent feature of climate change that is readily apparent in observations over recent decades [21]—making it the fastest-warming region on the Earth [1]. The four warmest years on record for the Arctic land have occurred in the last decade [18]. Indeed, the annual mass balance recorded for Aldegondabreen aligns closely with the regional temperature series, with four years of strongly negative values recorded since 2016 (Figure 1).
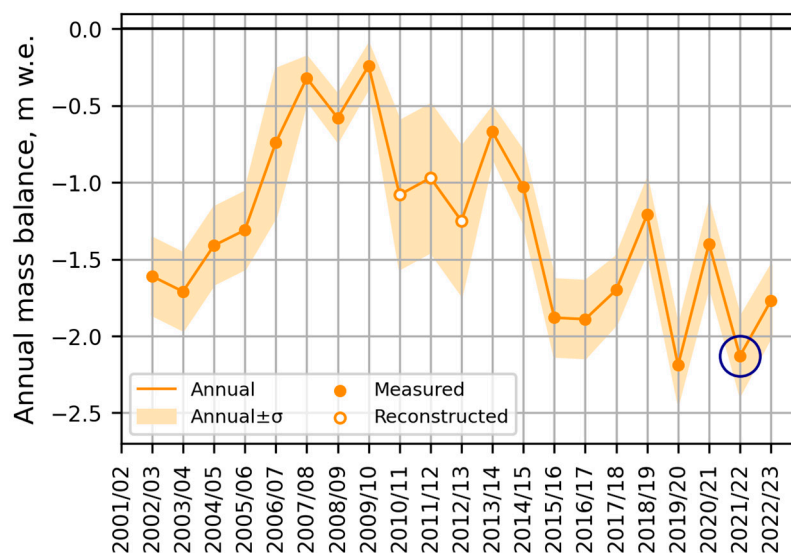
Figure 1. Aldegondabreen annual mass balance in the early 21st century. Blue circle highlights the mass-balance year studied in this paper.

Thus, the annual mass balance series reflects climatic fluctuations on at least a regional scale due to being synchronized with air temperatures. For example, between 2007 and 2020, the Pearson's coefficient between the annual mass balance (B_a) of Aldegondabreen and T_{6-9} (the mean air temperatures from June to September, which are typically the months with a positive mean air temperature in the Barentsburg area) was −0.81 [20]. The corresponding coefficient obtained from Ba and the annual positive degree–day sums was even higher at −0.84. In the balance year 2021/22, during which Svalbard experienced a record-breaking warm summer, the measured B_a value for Aldegondabreen was −2.13 ± 0.20 m w.e., which may be the highest glacier mass loss since the onset of monitoring [20] (Figure 1).

2.2. Heatwave Definition

A heatwave is a meteorological event that is defined as an extended period of unusually high atmosphere-related heat stress [22]. This definition is relatively broad and does not provide any quantitative means of identifying heatwaves. Different climatic and glaciological studies have used different approaches, including definitions based solely on thresholds of air temperature, which can either be symbolic round numbers (e.g., [13]) or derived from the statistical properties of the temporal distribution of temperature (e.g., [14]), as well as more complex definitions based on synoptic patterns [10]. This study adopts the statistics-driven approach and defines a heatwave as a period of consecutive days with daily mean air temperature anomalies exceeding the 90th percentile of that specific day in the 1991–2020 reference dataset [23]. Since the heatwaves are caused by synoptic-scale weather features that typically include those with lifetimes of a few days to a week or more [24,25], we only considered periods lasting for five days or more.

2.3. Model Overview

An energy balance model was developed based on the work of Wheler and Flowers [26], with several additional modifications. The model was run with a time step of one hour. The heat available for melt was computed for every grid cell from the surface energy balance equation, which is the sum of the absorbed solar radiation, longwave balance, sensible and latent heat turbulent fluxes, conductive (in-glacier) heat flux, and heat available for melt. The size of the grid cell was set to 30×30 m because that was the coarsest resolution of the input data derived from the Landsat imagery. The direction of all the energy fluxes in this study is considered to be relative to the glacier surface: fluxes that bring heat to the surface are positive, while those that carry heat away are negative.

The incoming solar radiative flux was computed with the ready-made "Potential Incoming Solar Radiation" module from the open-source "SAGA GIS" program and then scaled to real values [27]. The scaling coefficient was defined from real point measurements in the central, unshaded part of the glacier. Albedo maps derived from Landsat-8 imagery using equations from [28] were used to compute the absorbed solar radiation flux. Turbulent heat exchange was computed using the bulk aerodynamic method with parametrizations defined by [29], which are different for stable and unstable atmospheric conditions. The longwave balance was computed using an empirical equation proposed by [30] for Svalbard conditions. The conductive (in-glacier) energy flux was determined by employing a simple layered model introduced by [31], but with a larger number of subsurface layers rather than the two layers used in their study. The subsurface temperature profile was determined from the measurements made by a thermistor string drilled before the onset of melt. A more detailed description of the model can be found in [6].

2.4. Source Data

2.4.1. In Situ Weather Data

There are two permanently operational automatic weather stations (AWSs) on the Aldegondabreen glacier: one near the terminus and another in the upper reaches (Figures 2 and A1). These stations provided the model with air temperature, humidity, atmospheric pressure, wind speed, and solar radiation flux data. The differences in the values of the variables obtained at the two AWSs were used to compute vertical lapse rates, allowing for interpolation of the point measurements into distributed grids. Wind speed and cloud cover were assumed to be constant over the glacier at each time step because their interpolation requires the use of more complex models whose output cannot be verified.

An additional AWS was installed on the surface of the glacier close to its center between 2 August and 15 September 2022. This AWS carried a suite of sensors consisting of a CNR4 net radiometer (Kipp & Zonen, Delft, The Netherlands), a WindMaster 3D acoustic anemometer (Gill Instruments Limited, Hampshire, UK), and a 4.5 m deep GEOprecision thermistor string (GEOprecision GmbH, Ettlingen, Germany).

2.4.2. Eddy Covariance Measurements

These measurements were carried out on the Aldegondabreen glacier between 13 August and 3 September 2022 (21 days). The fluctuations in temperature T' and the three wind speed components u', v', and w' were measured using a WindMaster 3D anemometer at a height of 2 m above the surface and a frequency of 10 Hz. The sensible heat flux and the friction velocity were calculated by averaging the covariances between these variables over a 30 min window:

$$H = c_p \rho_a \overline{w' T'} \tag{1}$$

where ρ_a is the air density calculated based on the temperature and pressure, and c_p is the specific heat capacity of air (1010 J/(kg·K)).

The average wind speed u_z and the average temperature T_z, the covariance of vertical wind speed and temperature pulsations $\overline{w'T'}$, and the dynamic velocity u_* were calculated over each averaging interval:

$$u_* = \left(\overline{u'w'}^2 + \overline{v'w'}^2 \right)^{1/4} \tag{2}$$

The data acquired by this experiment were used to (1) compute the roughness parameters (z_{0m} and z_{0h}) of the glacier surface, which are used in the bulk aerodynamic equations, and (2) verify the sensible turbulent flux obtained from the bulk aerodynamic method.
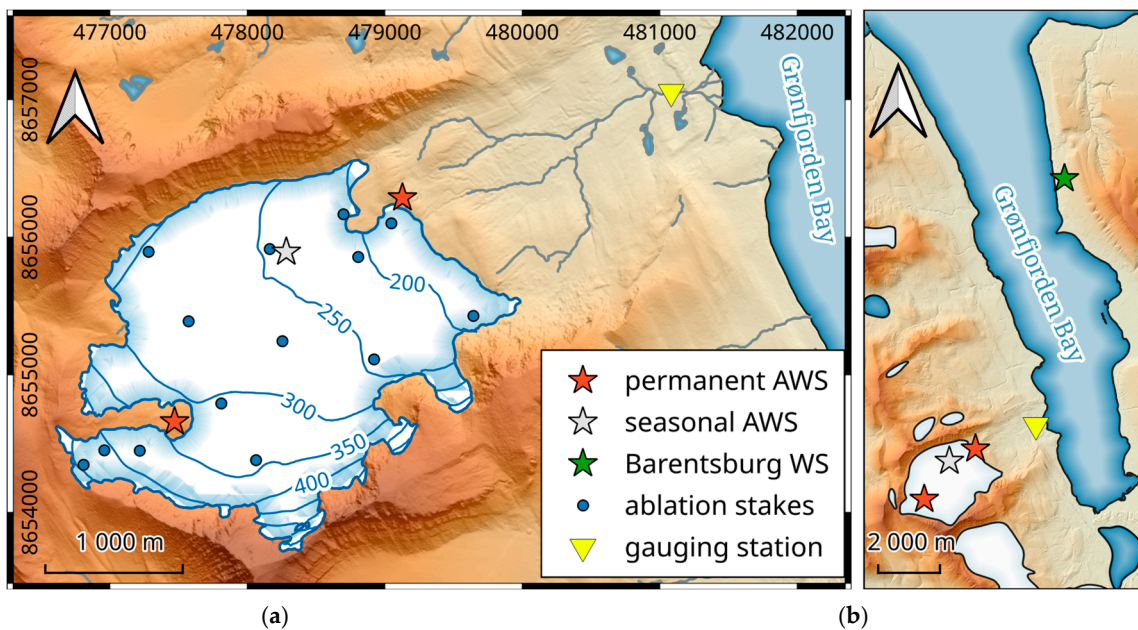
Figure 2. Measurement network (**a**) on the Aldegondabreen glacier in the summer of 2022; (**b**) Barentsburg weather station.

2.4.3. Climate Normals

Permanent weather observation stations were only established at Aldegondabreen in 2015; consequently, the computation of any climate normals from these data is not possible. Nevertheless, the obtained time series data extend far enough to demonstrate that the weather at Aldegondabreen and in Barentsburg are strongly correlated (Figure 3). This made it possible to develop linear regression models and recompute time series data obtained between 1991 and 2020 from the Barentsburg weather station into glacial data over the same time period (Equations (3)–(5)):

$$ws_A = 0.4312 \times ws_B + 1.6 \tag{3}$$

$$t2m_A = 1.1168 \times t2m_B - 0.1 \tag{4}$$

$$rh_A = 0.9402 \times rh_B - 3.3 \tag{5}$$

where ws and $t2m$ are the wind speed and air temperature at 2 m above the surface, respectively, and rh_A and rh_B are the relative humidity values of the Aldegondabreen glacier and Barentsburg town, respectively. From a physical perspective, these regressions effectively apply empirically found vertical lapses to the corresponding meteorological variables. Cloud cover data were used as is, without any recomputation; in particular, the

cloud cover was assumed to be constant across the ten kilometers separating the glacier and the Barentsburg weather station.
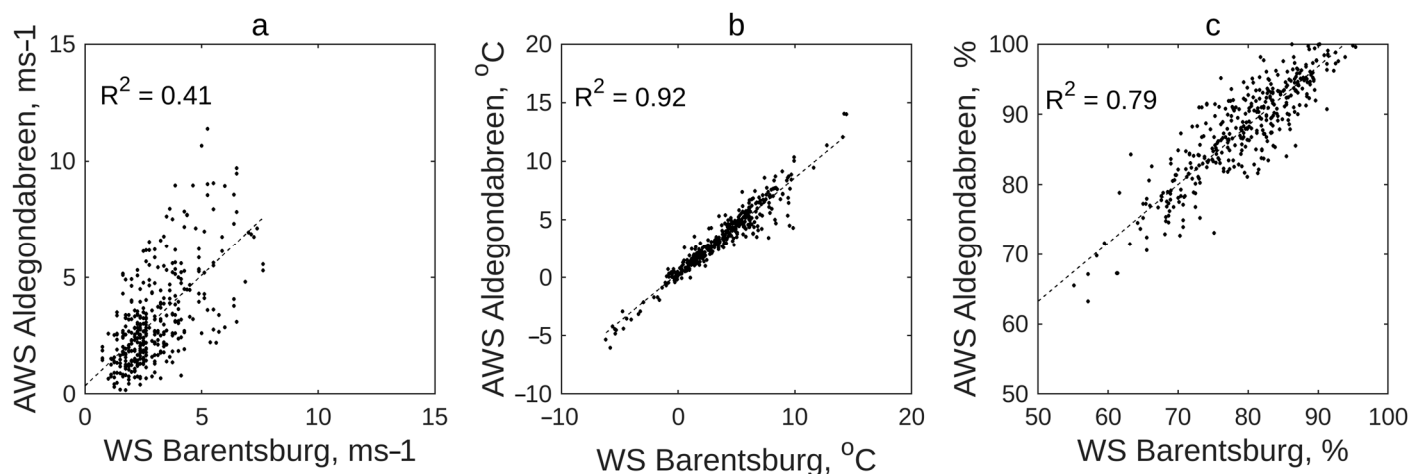
Figure 3. A comparison of the meteorological variables measured at the Barentsburg weather station and over the Aldegondabreen glacier from 15 May to 15 September in 2016–2022: (**a**) wind speed, (**b**) air temperature, (**c**) relative humidity.

The resulting thirty-year time series obtained for the Aldegondabreen glacier was then used to compute (1) turbulent fluxes using the bulk aerodynamic method and (2) the long-wave balance using the equation reported by Konig-Langlo and Augstein [30]. These computations involved two other variables that were impossible to derive from the data measured at Barentsburg: the glacier surface temperature and the near-surface air humidity.

2.4.4. Glaciological Mass Balance

The annual mass balance (B_a) of the Aldegondabreen glacier has been measured using the glaciological method since 2002/03 [20]. A total of 14 wooden ablation stakes have been distributed over the glacier surface to capture both elevation-related and lateral fluctuations in glacier mass balance. The annual mass balance is calculated using a floating-date time system with each balance year starting in the middle of September, when air temperatures become negative and solid precipitation begins. Typically, the stakes are visited and measured once every one or two weeks, as they need to be redrilled. At each ablation stake, the thickness of the ice melt layer computed from two consecutive readings is divided by the number of days between readings to obtain the ice melt rates in m w.e. day^{-1}.

The first stake measurement in the summer of 2022 occurred relatively late on 2 August. Following this, the stakes were visited every 5 to 7 days, resulting in 86 ice melt rate measurements that could be compared with the model outputs.

2.4.5. Proglacial Runoff

Several streams are known to originate from the Aldegondabreen glacier. These streams merge into a single river that flows into the Grønfjorden Bay. The total area of the watershed is 11.6 km^2, of which the glacier occupies about 5.2 km^2. During the summer seasons, the river is primarily fed by meltwater from the glacier [32]. An automated Solinst 3001 Levelogger gauge was installed about 1850 m downstream of the glacier terminus, allowing for the acquisition of water-level data from 8 June to 26 September 2022 at a frequency of 15 min. Near the gauging station, sixteen measurements of river discharge were carried out manually using the velocity–area method by utilizing an ISP-1M horizontal-axis hydrometric current meter. The resulting empirical equation allowed for the translation of water levels into discharge units.

To obtain the meltwater signal from the time series discharge data, we subtracted the atmospheric precipitation measured at the nearest gauge located in Barentsburg (10 km away); it was assumed that the rain was uniform over the entire watershed. No interpolation based on the vertical precipitation lapse was conducted, since this relationship was not known; no other precipitation gauges are located in the study area. The obvious drawback of such an approach is that it occasionally produces negative daily discharge values; these values were set to zero before further analyses.

3. SEB Modeling and Assessment

3.1. Comparison Between the Eddy Covariance and Bulk Aerodynamic Methods

The modeling of energy fluxes involves the use of several empirical coefficients that were adjusted during calibration. Although the total melt flux and the surface melt may have been modeled well, this does not guarantee that every single energy balance component was reproduced due to the phenomenon of model equifinality. Since this study primarily focused on turbulent fluxes, it was crucial to determine whether the modeling outputs were credible.

First, instead of assigning conventional values to the aerodynamic and thermal roughness parameters, which are needed for the bulk aerodynamic equations, these parameters were computed from the eddy covariance method. The estimated values were $z_{0m} = 0.8$ mm and $z_{0h} = 0.08$ mm. In glaciological studies, these parameters were often calibrated or just assumed to be certain rounded numbers in a reasonable range (e.g., [33–35]).

The sensible turbulent fluxes obtained from the two different methods were then compared. Values obtained from the bulk aerodynamic formulas performed well and did not demonstrate any significant biases (Figure 4); the difference in the time-averaged fluxes calculated over 21 days of observations (13 August to 3 September) was only 2 W m^{-2}. In the context of this study, the most important outcome of this comparison was that the uncertainty of the aerodynamic method was not dependent on the magnitude and direction of the wind speed or the flux value.
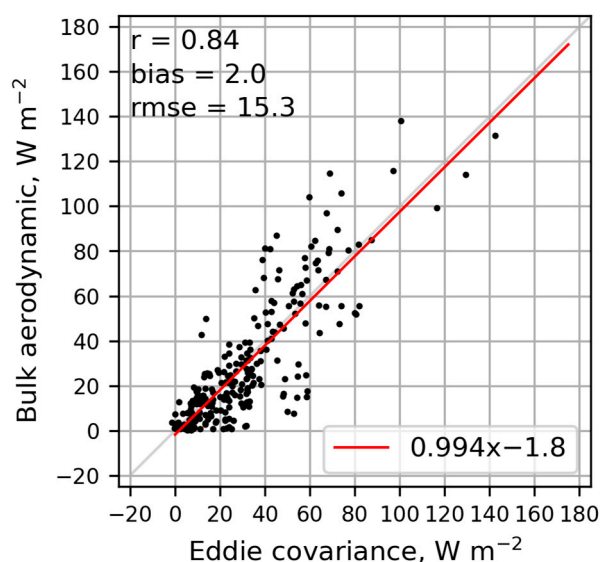
Figure 4. Comparison between the sensible turbulent flux values computed from the bulk aerodynamic method and eddy covariance observations at the Aldegondabreen glacier between 13 August and 3 September 2022.

3.2. Evaluation of Modeled Ice Melt Rates

The energy balance model was further evaluated using surface ice ablation data measured at the ablation stakes. The main criterion was how well the model represented the spatially distributed ice melt rates. A comparison between the modeled and observed ice melt rates revealed that $R^2 = 0.79$ and RMSE = 0.005 m w.e. (Figure 5a). The residuals were slightly asymmetrical; the median (*Mdn*) error was +0.7 mm w.e. day, indicating that the model was more likely to overestimate the total energy flux (Figure 5b).

(**a**)   (**b**)
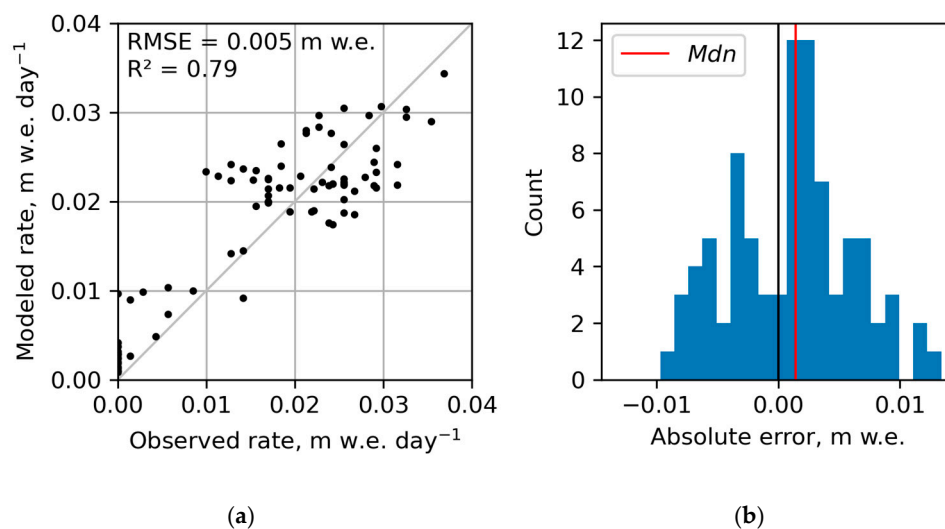
Figure 5. (**a**) Comparison between the modeled and measured melt rates of the Aldegondabreen glacier in summer–autumn 2022 (black line represents ideal match) and (**b**) distribution of the absolute errors (blue bars).

The demonstrated level of agreement with in situ observations was somewhat typical for glacier-scale SEB models [36]. Here, we consider the reported results to be good because the stake measurements themselves are not optimal; the review by Klug and co-authors [37] shows that the uncertainty of a stake reading may be as high as 2–3 cm due to stake inclination, stake sinking, or floating, among other factors. Given these uncertainties, as well as the rules of error propagation, the uncertainty of a measured melt layer was about 2.8 cm or ~2.4 cm w.e. Furthermore, the shorter the time between readings, the higher the uncertainty of the daily melt rates. In 2022, the typical periodicity of ablation measurements was about 7 days; consequently, the uncertainty of the daily melt rates was approximately $2.4/\sqrt{7} = 0.9$ cm day^{-1}, which is the same order of magnitude as the modeling uncertainty. Thus, achieving a lower RMSE for the model compared to the direct method does not have practical value since it requires more precise observation data for verification.

4. Results and Discussion

### 4.1. Impact of Heatwaves on the Energy Fluxes

The modeling outputs represent a time series of distributed energy fluxes over the Aldegondabreen glacier. The area-averaged daily values of these fluxes for the period between 1 May and 15 October are reported in Table 1. Shortwave solar radiation is known to be a primary energy source for the majority of glaciers worldwide [38,39], and this should also be true for Aldegondabreen, despite the frequently overcast weather conditions in Barentsburg. Due to its low elevation, the area of the accumulation zone at the present day has been effectively reduced to zero [20], and, during summer, the surface of this glacier is mainly covered by bare ice with an albedo of 0.2–0.4. Consequently, the glacier maintains a relatively low albedo during the summer and early autumn. However, the

ratio of turbulent heat exchange (38%) was found to be much higher than the one reported in studies of other low-elevation Svalbard glaciers [4,5,40] as well as previous observations on the Aldegondabreen glacier [6].

Table 1. Modeled surface energy balance values of Aldegondabreen from 1 May to 15 October 2022 and their ratios.

	Mean Flux; W m^{-2}	Ratio of Positive Components; %
Shortwave balance	65.4	68%
Sensible heat flux	25.9	27%
Latent heat flux	4.4	5%
Conductive heat flux	−4.9	—
Longwave balance	−12.2	—
Heat available for melt	78.5	—

Based on the definition of a heatwave adopted in this study, four distinct heatwaves were identified during the ablation season in 2022 (Figure 6), with the longest and most prominent occurring in May–June (19 days), two minor heatwaves in July and August (9 and 10 days, respectively), and a final heatwave in September–October (17 days).
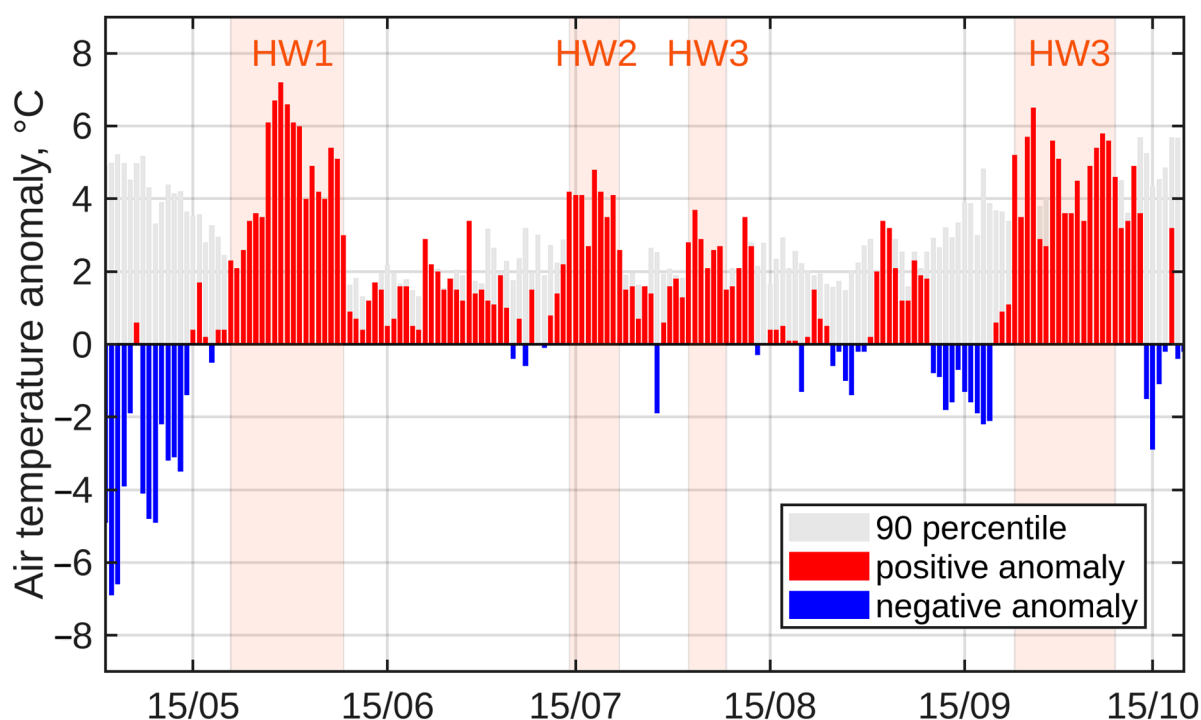
Figure 6. Air temperature anomalies in 2022 relative to the climatic normal of 1991–2020 and the four identified heatwaves. Grey bars represent the 90th percentile of the air temperature anomaly in 1991–2020.

During the first heatwave of 2022 (HW1), the turbulent heat exchange was 55.6 W m^{-2}, which was higher than its climatic normal in the 1991–2020 reference dataset (Table 2). Considering that the energy flux needed to melt 1 mm w.e. in a day is approximately 3.86 W m^{-2} and that the duration of HW1 was 19 days (roughly 1/10 of the entire ablation season), this represented 0.27 m w.e. of extra melt; in contrast, the measured B$_a$ for the same year was −2.13 m w.e.

Table 2. Surface energy flux anomalies at the Aldegondabreen glacier during the heatwaves identified in 2022 (relative to the climatic normals of 1991–2020).

Heatwave	Dates	Duration	Mean Anomaly, W m^{-2}		
			Sensible Heat Flux	Latent Heat Flux	Longwave Balance
HW1	21 May–08 June	19 days	+30.0	+25.6	6.1
HW2	14 July–22 July	9 days	−9.7	+7.0	−2.1
HW3	02 August–11 August	10 days	−14.4	+9.0	−13.6
HW4	23 September–09 October	17 days	+35.3	+24.8	+14.3

The contributions of the second and third heatwaves (HW2, HW3) are difficult to quantify. Although the air temperature exceeded the adopted threshold of the 90th percentile, there was no significant energy surplus based on the sum of the turbulent fluxes and the longwave balance (Table 2), which may seem contradictory. However, while air temperature is the primary driver of both turbulent heat exchange and the longwave balance, it is not the only factor that governs these processes. For example, the theory of turbulence states that sensible and latent heat fluxes are significantly amplified by wind speed. Similarly, longwave balance is also dependent on both air humidity and cloud cover.

The fourth heatwave (HW4) was estimated to have the greatest impact on the SEB of the Aldegondabreen glacier; the mean total anomaly of three heat balance components was approximately 66 W m^{-2}, which represents 0.33 m w.e. of extra melt. However, the actual melt should have been noticeably lower, as some amount of heat must be spent to warm up the glacier surface until the melt temperature is reached or to melt fresh solid precipitation; consequently, the reported value is considered to be an upper bound. The autumn melt was not measured directly at the ablation stakes, as the balance year and the stake observations ended on 15 September, after stake readings showed zero ablation over the last week, and the air temperature became negative. Consequently, according to the conventions of our glaciological monitoring program, the amount of melt recorded during the October thaw would be attributed to the mass balance of the following season (2022/23).

The main challenge in estimating the contribution of heatwaves to the SEB of the Aldegondabreen glacier is the difficulty of quantifying the effects of these phenomena on the shortwave solar radiation. Multiple studies have shown that heatwaves are typically associated with anticyclonic synoptic weather patterns (e.g., [10,24]). This suggests that heatwaves involve a reduction in cloud cover, which increases the shortwave radiation flux. This may have had an indirect effect on our data, as the anomalies of longwave balance, which are affected by low cloud cover, were negative during HW1–HW3. In contrast, during HW4 (which occurred in October), solar radiation would not have been significant even under clear-sky conditions, as the potential shortwave flux would have remained very low due to astronomical factors (polar night at this latitude starts in mid-November). Furthermore, there are no in situ observations of downwelling solar radiations before 2015 in the Barentsburg area, preventing us from calculating climatic normals for solar radiation. In addition, the use of reanalysis data would not allow for the computation of climatic normals of absorbed solar radiation, as there are no appropriate time series data for the Aldegondabreen albedo.
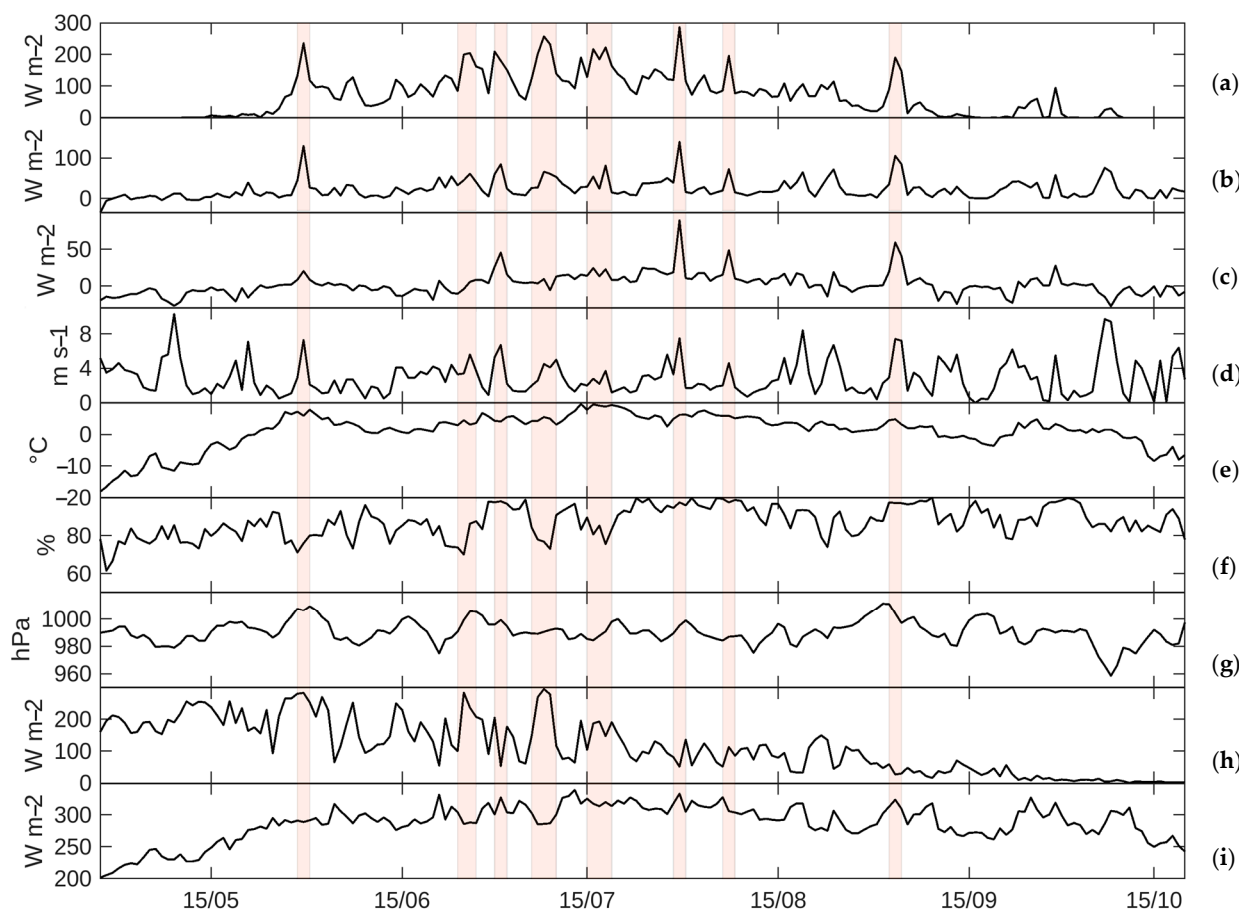
4.2. Extreme Melt Events

The modeling results suggest that, during the 2022 ablation season, there were several distinct peaks in the heat lasting for one to three consecutive days that would have been available for glacier melt. These peaks were not always associated with the heatwaves discussed above, though these events do coincide in some cases.

We treated all positive peaks in the modeled melt flux that exceeded the 90th percentile as extreme melt events. This statistical threshold was 49 mm w.e. day^{-1} in 2022 (corresponding to a melt flux of 189 W m^{-2}) over a total of 13 days, some of which were grouped into a single event. The dates for the eight identified extreme melt events are listed in Table 3. Notably, all the extreme melt events were observed on days with pronouncedly increased turbulent fluxes (Figure 7). On these dates, the glacier-averaged turbulent heat exchange increased by up to 140 and 90 W m^{-2} for the sensible and latent fluxes, respectively (Table 3).

Table 3. Extreme melt events for the Aldegondabreen glacier in 2022.

Dates	Duration, Days	Melt Rate; mm w.e. day^{-1}	Mean Sensible Flux; W m^{-2}	Mean Latent Flux; W m^{-2}
30 May	1	61	130.4	20.3
25–26 June	2	52	53.1	0.7
30 June	1	54	60.2	26.2
7–9 July	3	60	51.3	2.4
16–18 July	3	54	53.1	20.0
30 July	1	74	140.2	89.6
7 August	1	51	72.4	48.8
3 September	1	49	105.5	59.4

Figure 7. Weather conditions during the extreme melt events at the Aldegondabreen glacier in 2022: (**a**) melt flux; (**b**) sensible heat flux; (**c**) latent heat flux; (**d**) wind speed; (**e**) air temperature; (**f**) relative humidity; (**g**) atmospheric pressure at the AWS level; (**h**) shortwave solar radiation downward flux; and (**i**) longwave radiation downward flux.

On daily time scales, the modeled melt flux was best correlated with turbulent fluxes (Table 4). The most common weather conditions for all extreme melt events were increased wind and gust speed (Figure 7). Increases in wind speed were independent of the air temperature increases during the heatwaves, which amplifies daily ablation on days where extreme melt events and heatwaves coincide.

Table 4. Pairwise linear correlation matrix for the surface energy balance components of the Aldegondabreen glacier in 2022. Higher values are highlighted with green, lower values are in red.

|	QM	QH	QLE	SWD	LWD
Melt flux (QM)	-	0.69	0.68	0.34	0.58
Sensible heat flux (QH)	0.69	-	0.59	−0.03	0.45
Latent heat flux (QLE)	0.68	0.59	-	−0.12	0.63
Downwelling short-wave radiation (SWD)	0.34	−0.03	−0.12	-	−0.31
Downwelling longwave radiation (LWD)	0.58	0.45	0.63	−0.31	-

To assess the importance of the different meteorological variables on turbulent heat exchange, we used the dominance analysis technique proposed by Budescu [41] and Azen and Budescu [42] and implemented in the "dominance-analysis" package available in Python [43]. The determination of importance in this approach is based on multiple regression analysis and the identification of additional contributions of each predictor in all subset models. In cases where the target variable is continuous (e.g., sensible or latent turbulent heat flux), the package determines the dominance of one predictor over another by comparing their incremental R^2 contribution across all subset models. The results of the dominance analysis show that the most important factor in determining sensible heat flux in 2022 was wind speed, while the latent heat flux was most influenced by air temperature (Table 5).

Table 5. Importance of different meteorological variables to turbulent heat exchange flux during the 2022 melt season on the Aldegondabreen glacier.

	Sensible Heat Flux		Latent Heat Flux	
	Total Dominance; Dimensionless	Relative Importance; %	Total Dominance; Dimensionless	Relative Importance; %
Wind speed	0.50	65.9	0.01	2.7
Air temperature	0.24	31.0	0.24	49.2
Air humidity	0.01	1.4	0.17	35.0
Atmospheric pressure	0.01	1.3	0.05	9.8
Downwelling solar radiation	0.00	0.3	0.02	3.4

Water-level observations downstream of the glacier valley allowed for the automatic detection of daily mass balance variations (Figure 8a) that cannot be captured by the glaciological method. This is primarily due to the low temporal resolution of stake measurements, which are carried out weekly for logistical reasons, and partly due to stake reading uncertainties. To assess the relationship between the modeled surface melt and the observed stream discharge, the Spearman's rank correlation between the two datasets was computed (Figure 8b). There was a positive correlation between the two variables, $r(106) = 0.87$ ($p < 0.01$). This was considered to be relatively high due to the highly approximate subtraction of atmospheric precipitation from the time series of discharge. Although the hydrological measurements only provide lumped results, they demonstrate that the peaks in the turbulent fluxes observed in the model outputs did in fact exist and contributed

to the meltwater runoff and were not caused by excessive model sensitivity to some of the input variables.

(**a**)　　　　　　　　　　　　　　　　　　　　　　　(**b**)
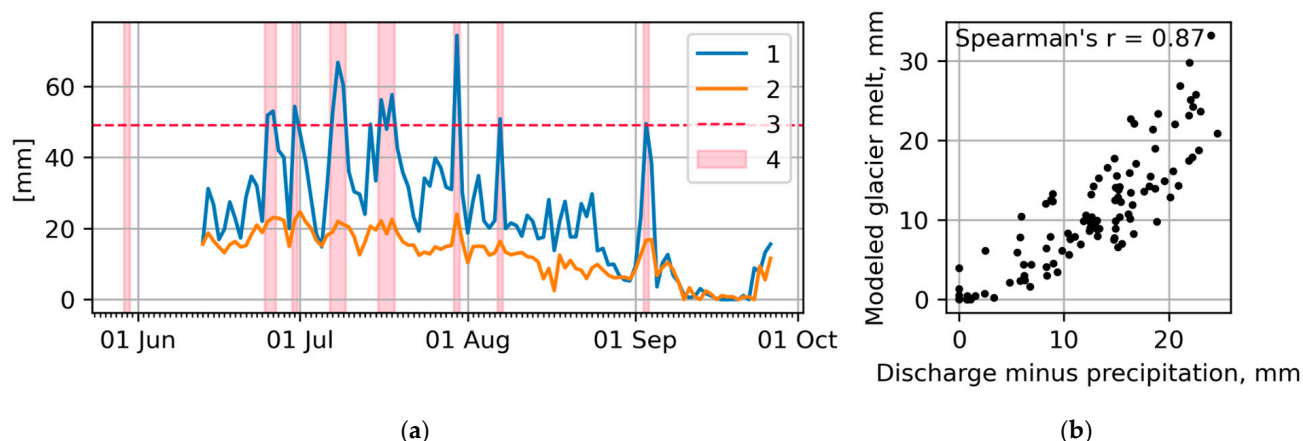
Figure 8. Comparison between (1) the glacier-averaged modeled melt layer at Aldegondabreen and (2) the downstream water runoff variations in 2022. The red dashed line (3) represents the 90th percentile of the modeled daily melt (49 mm w.e.), and periods (4) are the extreme melt events: (**a**) time series, (**b**) scatter plot.

We have, thus, demonstrated that air temperature is not the only factor that affects melt in low-elevation Svalbard glaciers. Turbulent fluxes may be significantly amplified by increased wind speeds, which then contribute to the amount of heat available for surface melt. Indeed, events in the Barentsburg area are independent of other types of extreme weather events, such as heatwaves, which can produce high daily melt rates (up to 75 mm w.e. of glacier-averaged melt per day) and affect proglacial runoff on a 1–3 day scale. At present, we cannot determine the impact of these shorter events on intra-annual time scales; however, extreme weather events are expected to occur more frequently and with increased duration [44]. Consequently, we recommend further research into the reproduction of these extreme weather events by models used for climatic forcings in projections of the Earth's glaciation.

5. Conclusions

In this study, we examined the surface mass and energy balance of the low-elevation Aldegondabreen glacier, as well as the intra-annual dynamics of the weather conditions in the area. The directly measured B_a in 2022 was one of the most negative values on record since the beginning of the century, while the ratio of turbulent fluxes in the SEB structure was anomalously high. We examined two types of extreme weather events that had an impact on the mass balance and the SEB. These phenomena differed in their duration; heatwaves had a lifespan of 9–19 days, while shorter extreme melt events only lasted for 1–3 days.

Four heatwaves were identified in 2022, defined as periods when the air temperature exceeded the 90th percentile of its climatic normal (based on a 1991–2020 reference dataset). During HW1, the turbulent heat exchange was 55.6 W m^{-2} higher than its climatic normal, equivalent to 0.27 m w.e. of extra melt. The contribution of the three other heatwaves was difficult to quantify; however, the most prominent heatwaves were observed in the spring and autumn, thus prolonging the ablation season for several weeks.

The effects of eight shorter extreme melt events, which were defined as periods exceeding the 90th percentile of the modeled energy available for glacier melt in 2022 (representing daily ablations of more than 49 mm w.e.), were observed in the form of positive peaks of stream discharge at the water-level gauge downstream of the Aldegondabreen glacier.

These events were characterized by increased wind speed (mean daily and hourly values of up to 10.3 m s^{-1} or 15.3 m s^{-1}, respectively), which dramatically amplified the turbulent heat exchange.

Heatwaves and other extreme weather events are likely to occur more frequently in the future due to ongoing climate changes. Our study shows that the events of different temporal scales may overlap to produce even more glacier melt. The results also emphasize that air temperature is not the only driver for some types of events, and a key question going forward is how well the weather conditions that drive these extreme melt events can be reproduced by models used for climatic forcing to allow for future projections of the Earth's cryosphere.

Data Availability Statement: The datasets presented in this article are not readily available because of the policy of the Arctic and Antarctic Research Institute (AARI), which does not allow us to make the field data publicly available. Requests to access the datasets should be directed to aaricoop@aari.ru.

Conflicts of Interest: The authors declare no conflict of interest.

Abbreviations

The following abbreviations are used in this manuscript:

Ba	Annual mass balance
AWS	Automated weather station
HW	Heatwave
RMSE	Root mean square error
w.e.	Water equivalent
SEB	Surface energy balance

Appendix A
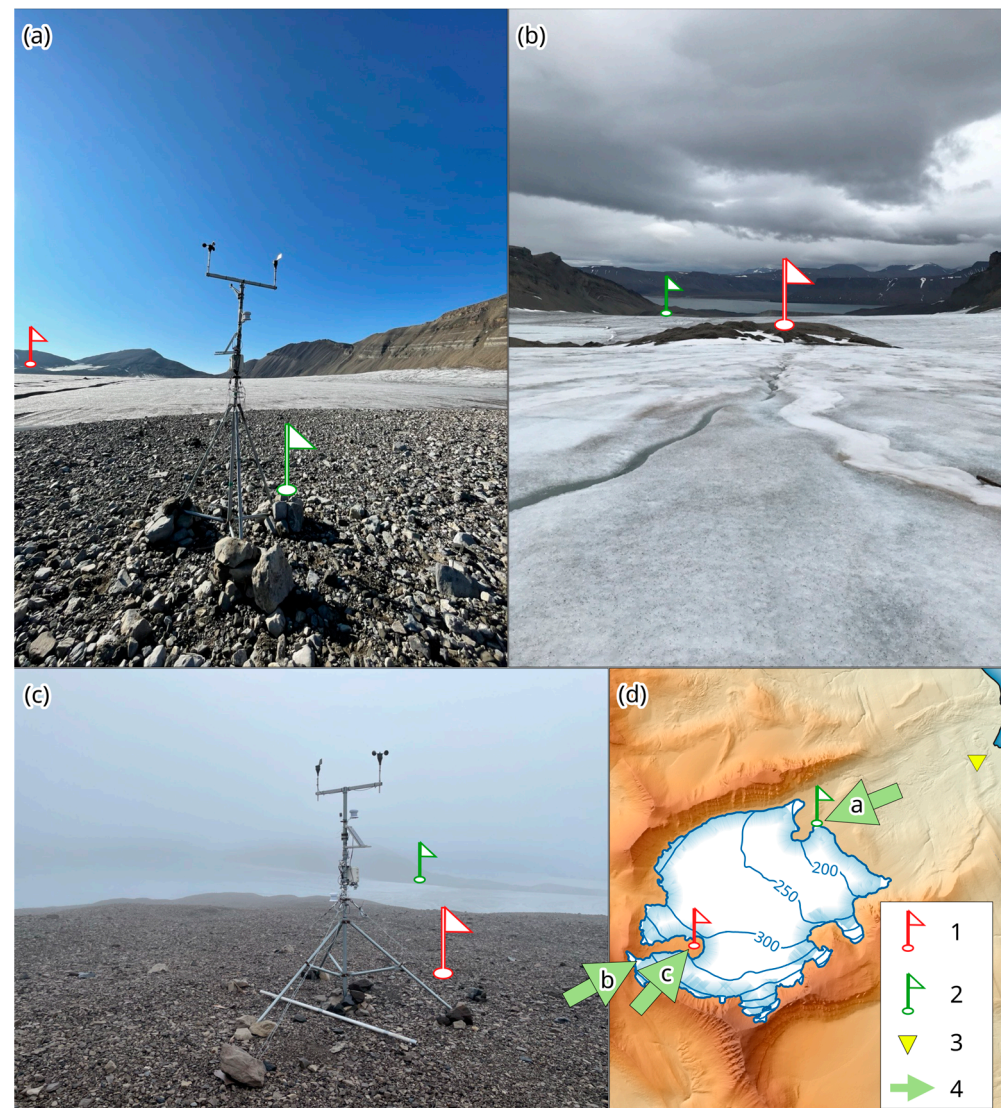
Figure A1. 1—upper weather station; 2—lower weather station; 3—gauging station; 4—location and the direction of the photos. Lower weather station (**a**), view from the top of the glacier (**b**), upper weather station (**c**), map with location and the direction of the photos a–c (**d**)

References

1. Isaksen, K.; Nordli, Ø.; Ivanov, B.; Køltzow, M.A.; Aaboe, S.; Gjelten, H.M.; Mezghani, A.; Eastwood, S.; Førland, E.; Benestad, R.E.; et al. Exceptional warming over the Barents area. *Sci. Rep.* **2022**, *12*, 9371. [CrossRef] [PubMed]
2. Schuler, T.V.; Kohler, J.; Elagina, N.; Hagen, J.O.M.; Hodson, A.J.; Jania, J.A.; Kääb, A.M.; Luks, B.; Małecki, J.; Moholdt, G.; et al. Reconciling Svalbard glacier mass balance. *Front. Earth Sci.* **2020**, *8*, 156. [CrossRef]
3. van Pelt, W.J.J.; Schuler, T.V.; Pohjola, V.A.; Pettersson, R. Accelerating future mass loss of Svalbard glaciers from a multi-model ensemble. *J. Glaciol.* **2021**, *67*, 485–499. [CrossRef]
4. Aas, K.S.; Dunse, T.; Collier, E.; Schuler, T.V.; Berntsen, T.K.; Kohler, J.; Luks, B. The climatic mass balance of Svalbard glaciers: A 10-year simulation with a coupled atmosphere–glacier mass balance model. *Cryosphere* **2016**, *10*, 1089–1104. [CrossRef]
5. Zou, X.; Ding, M.; Sun, W.; Yang, D.; Liu, W.; Huai, B.; Jin, S.; Xiao, C. The surface energy balance of Austre Lovénbreen, Svalbard, during the ablation period in 2014. *Polar Res.* **2020**, *40*. [CrossRef]
6. Prokhorova, U.; Terekhov, A.; Ivanov, B.; Demidov, V. Heat balance of a low-elevated Svalbard glacier during the ablation season: A case study of Aldegondabreen. *Arct. Antarct. Alp. Res.* **2023**, *55*, 2190057. [CrossRef]
7. Geyman, E.C.; van Pelt, W.J.J.; Maloof, A.C.; Aas, H.F.; Kohler, J. Historical glacier change on Svalbard predicts doubling of mass loss by 2100. *Nature* **2022**, *601*, 374–379. [CrossRef]

8. Karner, F.; Obleitner, F.; Krismer, T.; Kohler, J.; Greuell, W. A decade of energy and mass balance investigations on the glacier Kongsvegen, Svalbard. *J. Geophys. Res. Atmos.* **2013**, *118*, 3986–4000. [CrossRef]

9. Shestakova, A.A.; Chechin, D.G.; Lüpkes, C.; Hartmann, J.; Maturilli, M. The foehn effect during easterly flow over Svalbard. *Atmos. Chem. Phys.* **2022**, *22*, 1529–1548. [CrossRef]

10. Ventura, S.; Miró, J.R.; Peña, J.C.; Villalba, G. Analysis of synoptic weather patterns of heatwave events. *Clim. Dyn.* **2023**, *61*, 4679–4702. [CrossRef]

11. Hughes, P.D. Response of a Montenegro glacier to extreme summer heatwaves in 2003 and 2007. *Geogr. Ann. A Phys. Geogr.* **2008**, *90*, 259–267. [CrossRef]

12. Colucci, R.R.; Giorgi, F.; Torma, C. Unprecedented heat wave in December 2015 and potential for winter glacier ablation in the eastern Alps. *Sci. Rep.* **2017**, *7*, 7090. [CrossRef] [PubMed]

13. Cremona, A.; Huss, M.; Landmann, J.M.; Borner, J.; Farinotti, D. European heat waves 2022: Contribution to extreme glacier melt in Switzerland inferred from automated ablation readings. *Cryosphere* **2023**, *17*, 1895–1912. [CrossRef]

14. Chen, W.; Yao, T.; Zhang, G.; Woolway, R.I.; Yang, W.; Xu, F.; Zhou, T. Glacier surface heatwaves over the Tibetan Plateau. *Geophys. Res. Lett.* **2023**, *50*, e2022GL101115. [CrossRef]

15. Fisher, J.A.; Kochtitzky, W.H.; Edwards, B.R.; Irving, W.R.; Russell, K. Heat Wave Causes Major Melting Event in 2017 at 3 Glaciers Along the Lower Iskut River, British Columbia, Canada. In *AGU Fall Meeting Abstracts*; American Geophysical Union: Washington, DC, USA, 2018; C33D-1593. Available online: https://ui.adsabs.harvard.edu/abs/2018AGUFM.C33D1593F/abstract (accessed on 15 January 2025).

16. Pelto, M.S.; Dryak, M.; Pelto, J.; Matthews, T.; Perry, L.B. Contribution of Glacier Runoff during Heat Waves in the Nooksack River Basin USA. *Water* **2022**, *14*, 1145. [CrossRef]

17. Summer Melting in Svalbard. Available online: https://earthobservatory.nasa.gov/images/150165/summer-melting-in-svalbard (accessed on 21 December 2024).

18. Temperature 2022. Available online: https://climate.copernicus.eu/esotc/2022/arctic-temperature (accessed on 21 December 2024).

19. Noël, B.; Jakobs, C.L.; Van Pelt, W.J.J.; Lhermitte, S.; Wouters, B.; Kohler, J.; Hagen, J.O.; Luks, B.; Reijmer, C.H.; van de Berg, W.J.; et al. Low elevation of Svalbard glaciers drives high mass loss variability. *Nat. Commun.* **2020**, *11*, 4597. [CrossRef]

20. Terekhov, A.; Prokhorova, U.; Verkulich, S.; Demidov, V.; Sidorova, O.; Anisimov, M.; Romashova, K. Two decades of mass-balance observations on Aldegondabreen, Spitsbergen: Interannual variability and sensitivity to climate change. *Ann. Glaciol.* **2023**, *64*, 225–235. [CrossRef]

21. England, M.R.; Eisenman, I.; Lutsko, N.J.; Wagner, T.J.W. The recent emergence of Arctic Amplification. *Geophys. Res. Lett.* **2021**, *48*, e2021GL094086. [CrossRef]

22. Robinson, P.J. On the Definition of a Heat Wave. *J. Appl. Meteorol.* **2001**, *40*, 762–775. [CrossRef]

23. Hu, L.; Huang, G. The changes of high-temperature extremes and their links with atmospheric circulation over the Northern Hemisphere. *Theor. Appl. Climatol.* **2020**, *139*, 261–274. [CrossRef]

24. Kim, J.H.; Kim, S.J.; Kim, J.H.; Hayashi, M.; Kim, M.K. East Asian heatwaves driven by Arctic-Siberian warming. *Sci. Rep.* **2022**, *12*, 18025. [CrossRef] [PubMed]

25. Kim, D.S.; Jun, S.Y.; Lee, M.I.; Kug, J.S. Significant relationship between Arctic warming and East Asia hot summers. *Int. J. Climatol.* **2022**, *42*, 9530–9538. [CrossRef]

26. Wheler, B.A.; Flowers, G.E. Glacier subsurface heat-flux characterizations for energy-balance modelling in the Donjek Range, southwest Yukon, Canada. *J. Glaciol.* **2017**, *57*, 121–133. [CrossRef]

27. Böhner, J.; Antonić, O. Land-surface parameters specific to topo-climatology. *Dev. Soil Sci.* **2009**, *33*, 195–226. [CrossRef]

28. Naegeli, K.; Damm, A.; Huss, M.; Wulf, H.; Schaepman, M.; Hoelzle, M. Cross-comparison of albedo products for glacier surfaces derived from airborne and satellite (Sentinel-2 and Landsat 8) optical data. *J. Remote Sens.* **2017**, *9*, 110. [CrossRef]

29. Holtslag, A.A.M.; De Bruin, H.A.R. Applied modeling of the nighttime surface energy balance over land. *J. Appl. Meteorol. Clim.* **1988**, *27*, 689–704. [CrossRef]

30. König-Langlo, G.; Augstein, E. Parameterization of the downward long-wave radiation at the Earth's surface in polar regions. *Meteorol. Z.* **1994**, *3*, 343–347. [CrossRef]

31. Klok, E.L.; Oerlemans, J. Model study of the spatial distribution of the energy and mass balance of Morteratschgletscher, Switzerland. *J. Glaciol.* **2002**, *48*, 505–518. [CrossRef]

32. Romashova, K.V.; Chernov, R.A.; Vasilevich, I.I. Study of the glacial flow of rivers in the Grønfjord bay basin (Western Svalbard). *Arct. Antarct. Res.* **2019**, *65*, 34–45. [CrossRef]

33. Smeets, C.J.; Broeke, M.R. Temporal and spatial variations of the aerodynamic roughness length in the ablation zone of the Greenland ice sheet. *Bound. Lay. Meteorol.* **2008**, *128*, 315–338. [CrossRef]

34. Pel- licciotti, F.; Carenzo, M.; Helbing, J.; Rimkus, S.; Burlando, P. On the role of subsurface heat conduction in glacier energy-balance modelling. *Ann. Glaciol.* **2009**, *50*, 16–24. [CrossRef]

35. Covi, F.; Hock, R.; Reijmer, C.H. Challenges in modeling the energy balance and melt in the percolation zone of the Greenland ice sheet. *J. Glaciol.* **2023**, *69*, 164–178. [CrossRef]

36. Hill, T.; Dow, C.F.; Bash, E.A.; Copland, L. Application of an improved surface energy balance model to two large valley glaciers in the St. Elias Mountains, Yukon. *J. Glaciol.* **2021**, *67*, 297–312. [CrossRef]

37. Klug, C.; Bollmann, E.; Galos, S.P.; Nicholson, L.; Prinz, R.; Rieg, L.; Sailer, R.; Stötter, J.; Kaser, G. Geodetic reanalysis of annual glaciological mass balances (2001–2011) of Hintereisferner, Austria. *Cryosphere* **2018**, *12*, 833–849. [CrossRef]

38. Hock, R. Glacier melt: A review of processes and their modelling. *Prog. Phys. Geogr.* **2005**, *29*, 362–391. [CrossRef]

39. Smith, T.; Smith, M.W.; Chambers, J.R.; Sailer, R.; Nicholson, L.; Mertes, J.; Quincey, D.J.; Carrivick, J.L.; Stiperski, I. A scale-dependent model to represent changing aerodynamic roughness of ablating glacier ice based on repeat topographic surveys. *J. Glaciol.* **2020**, *66*, 950–964. [CrossRef]

40. Arnold, N.S.; Rees, W.G.; Hodson, A.J.; Kohler, J. Topographic controls on the surface energy balance of a high Arctic valley glacier. *J. Geophys. Res. Earth Surf.* **2006**, *111*, F02011. [CrossRef]

41. Budescu, D.V. Dominance analysis: A new approach to the problem of relative importance of predictors in multiple regression. *Psychol. Bull.* **1993**, *114*, 542–551. [CrossRef]

42. Azen, R.; Budescu, D.V. The Dominance Analysis Approach for Comparing Predictors in Multiple Regression. *Psychol. Methods* **2003**, *8*, 129–148. [CrossRef]

43. Dominance-analysis. Available online: https://github.com/dominance-analysis/dominance-analysis (accessed on 23 December 2024).

44. IPCC. 2021: Summary for Policymakers. In *Climate Change 2021: The Physical Science Basis. Contribution of Working Group I to the Sixth Assessment Report of the Intergovernmental Panel on Climate Change*; Masson-Delmotte, V., Zhai, P., Pirani, A., Connors, S.L., Péan, C., Berger, S., Caud, N., Chen, Y., Goldfarb, L., Gomis, M.I., et al., Eds.; Cambridge University Press: Cambridge, UK; New York, NY, USA, 2023; pp. 3–32. [CrossRef]